Article

Copyright © 2016 American Scientific Publishers
All rights reserved
Printed in the United States of America

Journal of
Nanoscience and Nanotechnology
Vol. 16, 709–714, 2016
www.aspbs.com/jnn

InN Quantum Dot Based Infra-Red Photodetectors

Arjun Shetty[1,*], Mahesh Kumar[2], Basanta Roul[3], K. J. Vinoy[1], and S. B. Krupanidhi[3]

[1] *Electrical Communication Engineering, Indian Institute of Science, Bangalore 560012, India*
[2] *Centre for Information and Communication Technology, Indian Institute of Technology Jodhpur, Jodhpur 342011, India*
[3] *Materials Research Centre, Indian Institute of Science, Bangalore 560012, India*

Self-assembled InN quantum dots (QDs) were grown on Si(111) substrate using plasma assisted molecular beam epitaxy (PA-MBE). Single-crystalline wurtzite structure of InN QDs was confirmed by X-ray diffraction. The dot densities were varied by varying the indium flux. Variation of dot density was confirmed by FESEM images. Interdigitated electrodes were fabricated using standard lithography steps to form metal-semiconductor-metal (MSM) photodetector devices. The devices show strong infrared response. It was found that the samples with higher density of InN QDs showed lower dark current and higher photo current. An explanation was provided for the observations and the experimental results were validated using Silvaco Atlas device simulator.

Keywords: Indium Nitride, Quantum Dots, IR Photodetector, Molecular Beam Epitaxy.

Delivered by Publishing Technology to: York University Libraries
IP: 206.214.3.16 On: Wed, ...
Copyright: American Scientific Publishers

1. INTRODUCTION

III-nitride semiconductors[1–3] have gained prominence in the past decade for their potential applications in optoelectronic devices like LEDs, solar cells and photodetectors.[4] III-nitride semiconductors are ideally suited for optoelectronic applications primarily due to their ability to form a continuous alloy system. Indium nitride has a high mobility, high saturation velocity, large drift velocity at room temperature and the smallest effective electron mass of all the group III-nitrides.[5–7] With advances in the growth of high quality InN using molecular beam epitaxy,[8–11] the fundamental bandgap of InN which was initially reported to be 1.9 eV[12] has been revised repeatedly and has now converged to a narrower value of 0.7 eV.[13,14] Consequently, III-nitride semiconductors have applications ranging from the UV[15] to the IR[16] region of the electromagnetic spectrum. By varying the fraction of In in $In_xGa_{1-x}N$ or by varying the fraction of Al in $Al_xGa_{1-x}N$, we can span a considerably wide range of bandgap from 0.7 to 6.2 eV that includes the technologically important solar spectrum. This makes III-nitrides a very attractive material system for solar cell applications. In addition to solar cells, another technologically significant optoelectronics application where III-nitrides can have a significant impact is reliable and high speed IR photodetectors for optical data communication. The proliferation of high speed optical data communication using fiber optics has given impetus to research in this direction especially to answer the question of whether these devices can be integrated with silicon optoelectronics. Approaches to integrate photodetectors with Si optoelectronics have included heteroepitaxial growth of elemental semiconductors like Ge on Si[17,18] as well as III–V semiconductors on Si.[19–21] The latter allows us to combine the high performance of silicon electronics with attractive optical properties of III–V semiconductors.

Amongst IR detectors, there has been increasing interest in quantum dot based infrared detectors.[22–24] The unique properties of semiconductor QDs have led to numerous studies on how these properties can be exploited for electronic and optoelectronic devices like lasers, photodetectors, light emitting diodes (LEDs), and field effect transistors (FETs). One of the advantages of quantum dot based detectors is that they are capable of operating at higher temperatures than other photodetectors.[24] The two primary methods used to fabricate self assembled III-nitride QDs are the Stranski-Krastanow (SK) growth mode and the droplet epitaxy technique.[25–32] In this work, use the SK growth mode to fabricated self assembled QDs of InN. Semiconductor crystallites with sizes of the order of a few nanometers exhibit optical and electrical properties that are different from those of the corresponding bulk material. Self assembled quantum dots are particularly suited for IR photodetector applications due to advantages

*Author to whom correspondence should be addressed.

 1533-4880/2016/16/709/006 doi:10.1166/jnn.2016.10679

like intrinsic sensitivity to normally incident IR light and longer lifetime of excited electrons due to greatly suppressed electron-phonon scattering.[33] Among the various photodetector structures, the planar metal-semiconductor-metal (MSM) structure has advantages like ease of fabrication, inherently low capacitance and consequently, greater receiver sensitivity as compared to other vertically structured photodetectors.[34]

This work studies the IR photoresponse of self assembled InN quantum dots on Si substrate in a MSM photodetector configuration. In particular, we study the effect of quantum dot density on the performance parameters of the photodetector device like photocurrent to dark current ratio. It is important to study and to understand how various growth parameters affect the photoresponse properties in this material system before adopting it for optoelectronic applications.

2. EXPERIMENTAL DETAILS

Samples used in our experiments were grown on undoped Si(111) (resistivity >3000 Ω cm) substrates using a plasma assisted molecular beam epitaxy (PAMBE) system (OMICRON) equipped with a radio frequency (RF) plasma source. The base pressure in the system was lower than 1×10^{-10} mbar. The Si substrates were first ultrasonically cleaned in isopropyl alcohol (IPA) for 10 mins. This was followed by boiling in trichloroethylene, acetone and methanol at 70 °C for 5 min each. These boiling steps are repeated for 2 more rounds. This was followed by a dip in dilute HF (5%) to remove the native oxide on Si. The Si sample was then loaded into the growth chamber and outgassed at 900 °C for 1 h. The growth conditions comprise parameters like substrate temperature, indium flux (beam equivalent pressure), nitrogen flow rate and RF plasma power. The InN QD samples were grown at a substrate temperature of 410 °C with different indium beam equivalent pressures (BEP). The indium BEP for the three samples (a), (b) and (c) were kept 5.32×10^{-8}, 8.36×10^{-8}, and 1.35×10^{-7} mbar, respectively. The indium flux is varied by changing the temperature of the indium effusion cell to previously calibrated values. Nitrogen flow rate and plasma power were kept at 0.5 sccm (sccm denotes standard cubic centimeter per minute at standard temperature and pressure) and 350 W, respectively for all the samples. The structural and morphological characterizations were carried out by using X-ray diffractometer and field effect scanning electron microscope (FESEM). Interdigited electrode pattern was formed on the samples by standard UV photolithography using AZ5214 photoresist and an EVG 620 double sided mask aligner. This was followed by metal (Al) deposition using thermal evaporation. Liftoff was performed by placing the samples in acetone. Al interdigited electrode structures were formed with a finger spacing and finger width of 10 μm. The dark and photocurrent measurements were made using a probe station attached to an

Delivered by Publishing Technology to

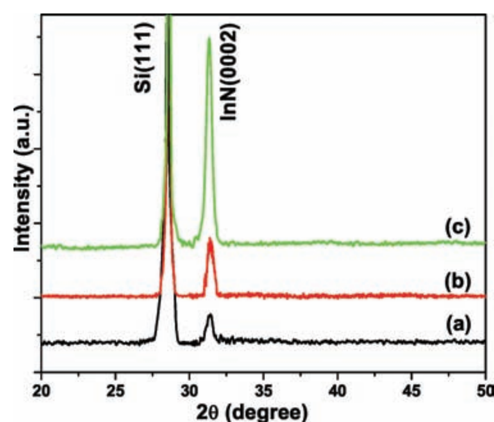

Figure 1. XRD of InN quantum dots on Si substrate.

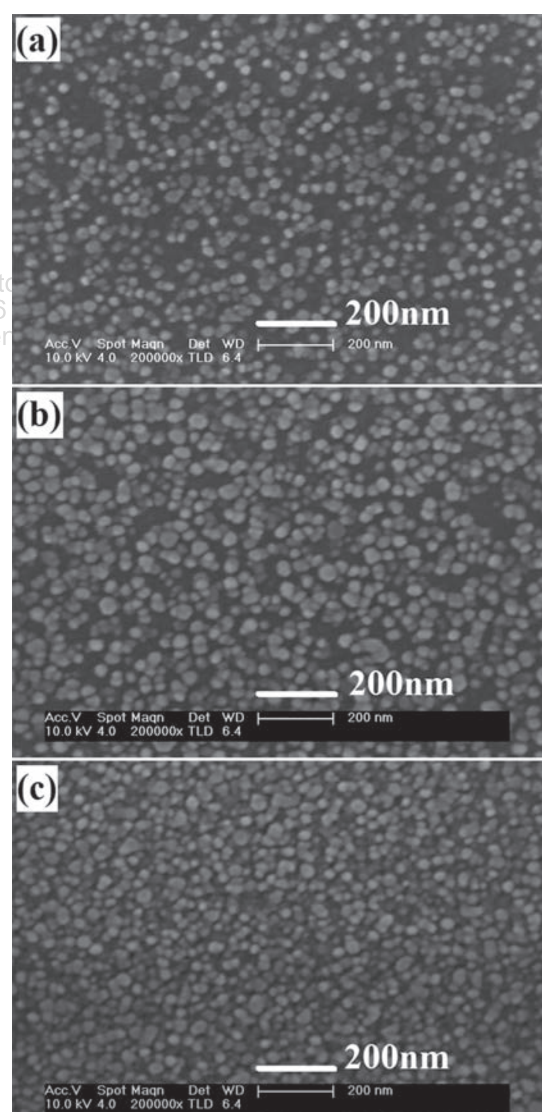

Figure 2. SEM Image of InN quantum dots of varying dot density (a) 5.32×10^{-8} cm^{-2} (b) 8.36×10^{-8} cm^{-2} (c) 1.35×10^{-7} cm^{-2}.

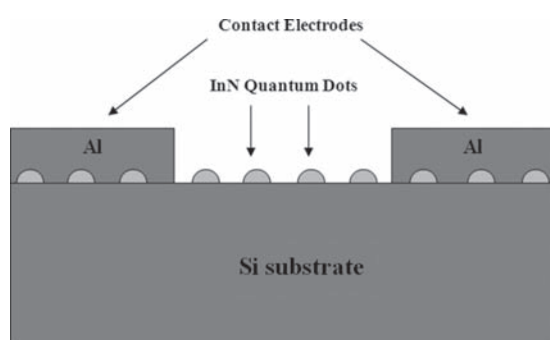

Figure 3. Schematic structure of InN quantum dot MSM photodetector.

Agilent Device Analyzer B1500A. In this work, we focus on demonstrating how a change in indium flux results in variation in QD density and how this variation of QD density affects the infrared (IR) photo response demonstrated by the three samples along with explanations for the observations.

3. RESULTS AND DISCUSSION

There were two primary goals of this study. The first was to study the effect of varying indium flux on the MBE grown InN QD size and density. The second was to study the effect of varying QD density on IR photodetector performance. The characterization techniques used to achieve the first goal were XRD and FESEM. Formation of InN QDs was confirmed by XRD and variation of density was observed *ex-situ* using FESEM. The second goal was achieved by fabricating intedigited electrodes and forming MSM photodetectors and studying their dark and photocurrent characteristics. The photodetector experimental results were validated using simulations in Silvaco Atlas.

Confirmations on the formation of InN and structural characterizations of the as-grown samples were carried out by high-resolution X-ray diffraction (HRXRD). The XRD 2θ-ω scan of InN QDs are shown in Figure 1. The peaks corresponding to Si(111) substrate ($\theta = 28.48°$) and InN (0002) ($\theta = 31.38°$) are clearly seen. This confirms that the InN QDs are grown along [0002] direction of wurtzite hexagonal structure of InN.

Delivered by Publishing Technology to: York University Libraries
Copyright: American Scientific Publishers

The SEM images of the three grown samples (a), (b) and (c) are shown in Figure 2. The density of the hence formed QDs showed significant variation with the change in beam equivalent pressure of In cell which was controlled by the temperature of the In effusion cell. From the figure it can be seen that increasing the BEP of In has resulted in an increase in QDs density while the average size of quantum dots has remained almost the same. The average size of the QDs is found to be 25 nm $\pm$ 2 nm. By changing the BEP from 5.32×10^{-8} mbar to 1.35×10^{-7} mbar, there is a substantial and consistent variation in the QD density from 5.3×10^{10} cm^{-2} to 7.75×10^{10} cm^{-2}.

Figure 3 shows the schematic diagram of the fabricated device. Ideally we would prefer to have a Schottky contact between metal and InN and reduce dark currents for the metal-semiconductor-metal interdigited electrode photodetector structure. However, due to the high carrier concentrations associated with InN, it is not possible to obtain a Schottky contact between metal and InN. Al is used as the metal for the electrodes and it makes an ohmic contact with InN. Photodetector structures were successfully fabricated on the samples by standard photolithography followed by metal (Al) deposition and liftoff to create the interdigited electrode structures with a finger spacing and finger width of 10 μm.

Figure 4 shows the optical image of the electrode pattern for the photodetectors. The finger widths and finger spacings are 10 μm. The length of the finger is 1 mm. The overall active device area covered by the interdigited electrodes is 1 mm by 1 mm. Two contact pads of 1 mm by 1 mm are provided on either ends of the fingers to probe the device. Photo responsive studies were made on the fabricated photodetector structures in the presence of IR radiation and under dark conditions. A Phillips IR lamp with a power of 100 W was used as the broadband source of IR radiation.

Figure 5 shows the plot of dark and photo current versus applied voltage for the three InN QD samples and a bare Si substrate. All InN QD samples produce lower dark current as compared to the bare Si sample. We observe that as the density of QDs increases (sample (a) to sample (c)), there is a decrease in the dark current. The decrease in

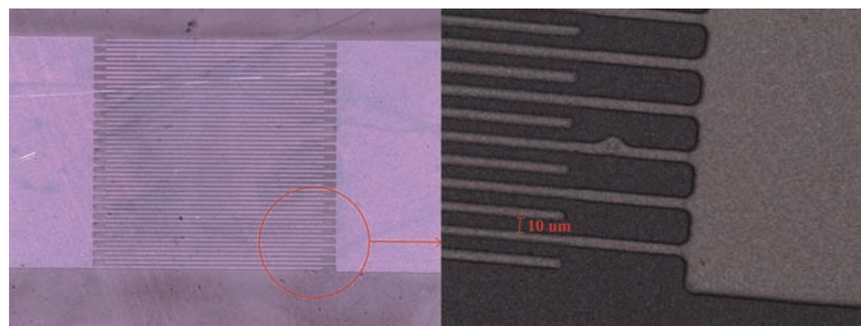

Figure 4. Optical microscope image of fabricated interdigitated electrodes (finger width = finger spacing = 10 μm).

dark current in the case of InN samples indicates that the presence of InN quantum dots beneath the Al electrodes reduces current between the fingers of the interdigited electrodes.[35] This is because, in the presence of quantum dots under the electrodes, the carriers have to cross two interfaces namely, Al/InN interface and InN/Si interface. As the density of quantum dots increases, the fraction of area under the electrodes covered by InN increases. As a result, greater numbers of carriers are forced to traverse the difficult Al/InN and InN/Si interfaces as compared to the easier path of traversing only the Al/Si interface. This results in a decrease in dark current with increase in density of InN quantum dots. Similar behaviour has been reported in literature for InGaN quantum dots on Si[35] and Ge islands on Si.[36]

Also, all InN QD samples produce higher photo current as compared to the bare Si sample. It is observed that as the density of quantum dots increases, there is an increase in the photocurrent. The observed increase in photocurrent with increase in quantum dot density can be attributed to the increased IR absorption along with the increase in quantum dot density. Figure 6 shows the plot of variation of dark current and photo current to dark current ratio with dot density. The summary of our results consisting of the variation of QD density with indium flux and the resulting dependence of photodetector performance on QD density is given in Table I.

Delivered by Publishing Technology to: York University Libraries
IP: ... On: Wed, 06 Jan 2016 06:28:16
Copyright: American Scientific Publishers

The results have been validated with simulation using Silvao Atals device simulator. The device structure of Figure 3 was created and modelled in 2D in Silvaco Atlas. Semiconductor properties like bandgap and carrier mobilty for InN and Si were taken from the inbuilt material library of Silvaco. As shown in Figure 3, the quantum dots were simulated by taking rectangular shaped islands of InN embedded within the Si block. The width of the block was taken to be 25 nm corresponding to the average diameter of the quantum dot. The variation of the quantum dot density of was modelled by making sure that the number of rectangular InN islands included in a particular simulation were relatively proportional to the QD density in the sample being modelled. The resulting dark current showed a similar trend as that shown by our experimental results. Increasing InN quantum dot density resulted in a decrease in dark current as shown in Figure 7. Photo currents were not measured as it was not feasible to expect the simulation setup to include all the various effects of the practical device especially in the presence of such a random distribution of self assembled QDs. For the same reason, the dark current simulation values do not exactly match the experimentally measured dark current values. The purpose of the simulation was to demonstrate the trend of increasing dot density leading to decreasing dark current and this has been demonstrated as shown in Figure 7.

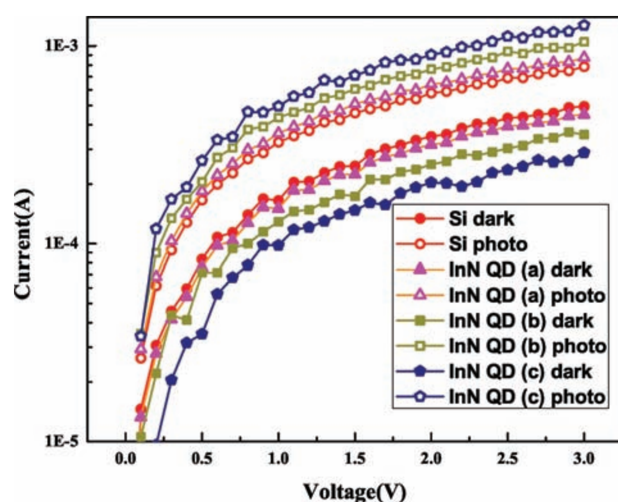

Figure 5. Experimentally measured dark and photocurrent response of bare Si photodetector and InN QD photodetectors.

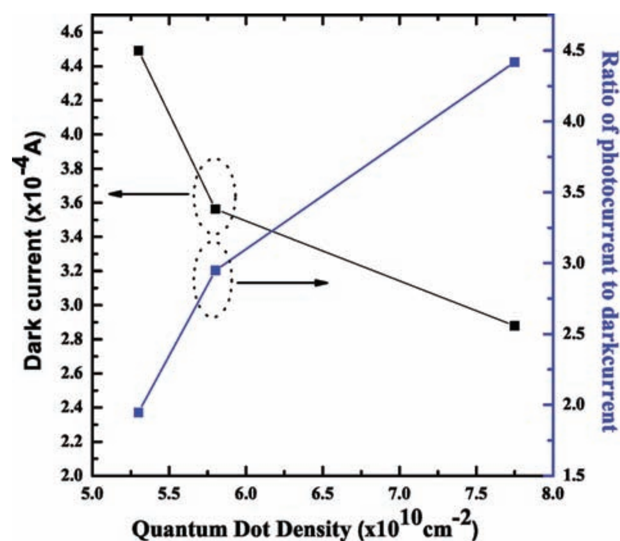

Figure 6. Variation of dark current and photocurrent to dark current ratio with quantum dot density.

The experimental transient response curve of the photodetector (sample (c)) has been shown in Figure 8. These results were plotted by applying a bias of 3 V and turning the IR lamp on and off. The time constants involved in the on-off transient response of the photodetector were determined. The decay part of the transient response curve (when the lamp was switched from on to off) was fitted to

$$I(t) = I_{\text{dark}} + A\exp\left\{\frac{-(t-t_0)}{\tau}\right\} \tag{1}$$

Table I. Comparision of sample parameters.

Sample	Indium BEP (mbar)	QD density (cm^{-2})	Dark current (mA)	Ratio of photocurrent to dark current (at 3 V bias)
(a)	5.32×10^{-8}	5.3×10^{10}	0.449	1.95
(b)	8.36×10^{-8}	5.8×10^{10}	0.356	2.95
(c)	1.35×10^{-7}	7.75×10^{10}	0.288	4.42

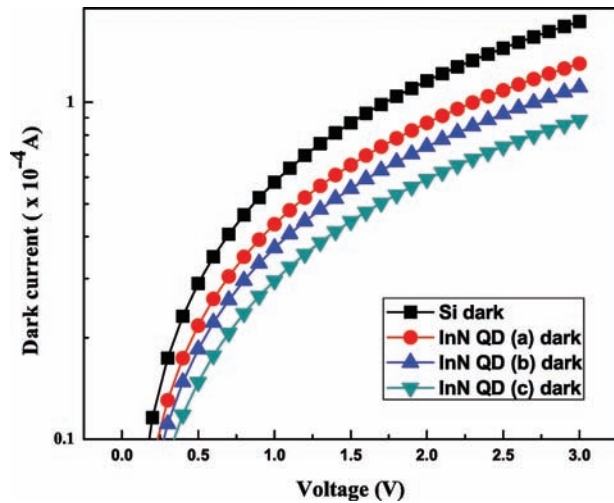

Figure 7. Simulated dark current of bare Si photodetector and InN QD photodetectors.

and the rise part of the transient response curve (when the lamp was switched from off to on) was fitted to

$$I(t) = I_{\text{dark}} + A\left[1 - \exp\left\{\frac{-(t-t_0)}{\tau}\right\}\right] \tag{2}$$

Here, $A = (I_{\text{photo}} - I_{\text{dark}})$ is the scaling constant, I_{photo} is the steady state photocurrent, I_{dark} is the steady state dark current, τ is the corresponding time constant and t_0 is the time at which the lamp is turned on or off. The average decay time constant was found to be 1.22 s and the average rise time constant was found to be 1.43 s. It is seen that the dynamic response of the device is stable and reproducible and it can be used for IR photodetector applications.

The present study shows that increase in BEP during growth of self assembled InN QDs results in higher dot density which in turn results in lower dark current and higher photocurrent in fabricated IR photodetectors. These results indicate the growth parameters that result in better quality IR photodetectors for the epitaxial growth of a III–V semiconductor on Si and this might lead to better quality photodetectors for applications that require a combination of the low cost of Si electronics with the attractive optoelectronics of III–V semiconductors.

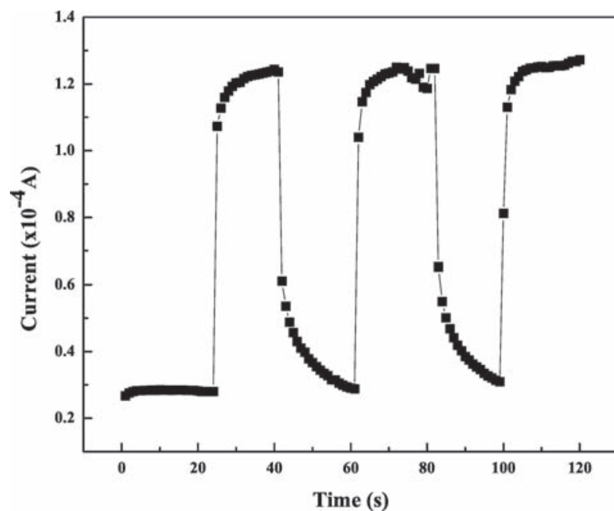

Figure 8. Experimentally measured transient response.

4. CONCLUSIONS

InN quantum dots of varying dot densities were grown on Si substrates using molecular beam epitaxy. Metal-semiconductor-metal photodetector structures were fabricated using standard lithography steps. Dark and photocurrent measurements were carried out on the samples. We observed that an increase in quantum dot density results in a decrease in dark current and an increase in photocurrent. Overall, the increasing density of QDs results in an improvement of the photocurrent to dark current ratio of the photodetector. The decrease in dark current has resulted from the increase in the fraction of carriers that have to cross two barriers: metal-InN and InN-Si as compared to just the metal-Si barrier. The increase in photocurrent with density is possibly due to the increase in number of photocarriers generated in InN which add up to the photocarriers generated in Si. The results have been validated using industry standard device simulator Silvaco Atlas and we observe sufficient agreement between them to support our experimental results.

Delivered by Publishing Technology
IP: 206.214.3.16 On: Wed, 06 Jan 2016 06:28:16
Copyright: American Scientific Publishers

References and Notes

1. S. C. Jain, M. Willander, J. Narayan, and R. V. Overstraeten, *J. Appl. Phys.* 87, 965 (**2000**).
2. O. Ambacher, *J. Phys. D: Appl. Phys.* 31.20, 2653 (**1999**).
3. H. J. Quah and K. Y. Cheong, *Sci. Adv. Mater.* 5, 1816 (**2013**).
4. R. F. Davis, *Proceedings of the IEEE* 79.5, 702 (**1991**).
5. S. N. Mohammad and H. Morkoc, *Prog. Quantum Electron* 20, 361 (**1996**).
6. E. Bellotti, B. F. Brennan, J. D. Albrecht, and L. F. Eastman *J. Appl. Phys.* 85, 916 (**1999**).
7. S. K. O'Leary, B. E. Foutz, M. S. Shur, U. V. Bhapkar, and L. F. Eastman, *J. Appl. Phys.* 83, 826 (**1997**).
8. H. Lu, W. J. Schaff, J. Hwang, H. Wu, G. Koley, and L. F. Eastman, *Appl. Phys. Lett.* 79, 1489 (**2001**).
9. Y. V. Davydov, A. A. Klochikhin, R. P. Seisyan, V. V. Emtsev, S. V. Ivanov, F. Bechstedt, J. Furthmuller, H. Harima, A. V. Mudryi, J. Aderhold, O. Semchinova, and J. Graul, *Physica Status Solidi (b)* 229, r1-r3 (**2002**).
10. Y. Nanishi, Y. Saito, and T. Yamaguchi, *Jpn. J. Appl. Phys., Part 1* 42, 2549 (**2003**).
11. K. H. Lee, S. P. Chang, K. W. Liu, P. C. Chang, S. J. Chang, T. P. Chen, H. W. Shiu, L. Y. Chang, and C. H. Chen, *Sci. Adv. Mater.* 5, 873 (**2013**).
12. T. L. Tansley and C. P. Foley, *J. Appl. Phys.* 59.9, 3241 (**1986**).
13. J. Wu, W. Walukiewicz, W. Shan, K. M. Yu, J. W. Ager III, E. E. Haller, H. Lu, and W. J. Schaff, *Physical Review B* 66, 201403 (**2002**).
14. J. Wu, W. Walukiewicz, W. Shan, K. M. Yu, J. W. Ager III, S. X. Li, E. E. Haller, H. Lu, and W. J. Schaff, *J. Appl. Phys.* 94, 4457 (**2003**).
15. E. Munoz, E. Monroy, J. L. Pau, F. Calle, F. Omnes, and P. Gibart, *J. Phys.: Condens. Matter* 13, 7115 (**2001**).

16. J. Wu, *J. Appl. Phys.* 106.1, 011101 (**2009**).

17. L. Colace, G. Masini, and G. Assanto, *Quantum Electronics, IEEE Journal* 35.12, 1843 (**1999**).

18. A. S. Z. Othaman, S. K. Ghoshal, S. S. Lapari, and N. Pourmand, *Nanosci. Nanotechnol. Lett.* 6, 106 (**2014**).

19. E. Droge, R. F. Schnabel, E. H. Bottcher, M. Grundmann, A. Krost, and D. B. Droge, *Electron. Lett* 30.16, 1348 (**1994**).

20. C. Junesand, M. H. Gau, Y. T. Sun, S. Lourdudoss, I. Lo, J. Jimenez, P. A. Postigo, F. M. Morales, J. Hernandez, S. Molina, A. Abdessamad, G. Pozina, L. Hultman, and P. Pirouz, *Mater. Express* 4, 41 (**2014**).

21. V. N. Singh, G. Partheepan, B. Kumar and A. Khare, *Mater. Express* 3, 360 (**2013**).

22. J. Phillips, K. Kamath, and P. Bhattacharya, *Appl. Phys. Lett.* 72.16, 2020 (**1998**).

23. S. J. Xu, S. J. Chua, T. Mei, X. C. Wang, X. H. Zhang, G. Karunasiri, W. J. Fan, C. H. Wang, J. Jiang, S. Wang, and X. G. Xie, *Appl. Phys. Lett.* 73, 3153 (**1998**).

24. Y. H. Kang, J. Park, U. H. Lee, and S. Hong, *Appl. Phys. Lett.* 82.7, 1099 (**2003**).

25. B. Daudin, F. Widmann, G. Feuillet, Y. Samson, M. Arlery, and J. L. Rouviere, *Phys. Rev. B* 56, R7069 (**1997**).

26. C. Adelmann, N. Gogneau, E. Sarigiannidou, J. L. Rouviere, and B. Daudin, *Appl. Phys. Lett.* 81, 3064 (**2002**).

27. N. Koguchi and K. Ishige, *Jpn. J. Appl. Phys.* 32, 2052 (**1993**).

28. C. W. Hu, A. Bell, F. A. Ponce, D. J. Smith, and I. S. T. Tsong, *Appl. Phys. Lett.* 81, 3236 (**2002**).

29. B. Chitara, D. S. I. Jebakumar, C. N. R. Rao, and S. B. Krupanidhi, *Nano-Technology* 20, 405205 (**2009**).

30. K. Kawasaki, D. Yamazaki, A. Kinoshita, H. Hirayama, K. Tsutsui, and Y. Aoyagi, *Appl. Phys. Lett.* 79, 2243 (**2001**).

31. T. Maruyama, H. Otsubo, T. Kondo, Y. Yamamotob, and S. Naritsuka, *J. Cryst. Growth* 301/302, 486 (**2007**).

32. W. C. Ke and W. C. Houng, *Sci. Adv. Mater.* 5, 137 (**2013**).

33. Z. Chen, E. T. Kim, and A. Madhukar, *Appl. Phys. Lett.* 80.14, 2490 (**2002**).

34. D. L. Rogers, *Lightwave Technology, Journal of* 9.12, 1635 (**1991**).

35. L. W. Ji, Y. K. Su, S. J. Chang, S. H. Liu, C. K. Wang, S. T. Tsai, T. H. Fang, L. W. Wu, and Q. K. Xue, *Solid-State Electron* 47, 1753 (**2003**).

36. A. Baharin and M. R. Hashim, *Semicond. Sci. Technol.* 22, 905 (**2007**).

Received: 20 September 2014. Accepted: 24 October 2014.

Delivered by Publishing Technology to: York University Libraries
IP: 206.214.3.16 On: Wed, 06 Jan 2016 06:28:16
Copyright: American Scientific Publishers